Desalination and Water Treatment
www.deswater.com

doi: 10.5004/dwt.2019.23499

142 (2019) 24–36
February

Comparison of energy-efficient configurations of direct-contact membrane distillation for brackish water desalination

Emad Ali[a,*], Jamel Orfi[b], Abdullah Najib[b], Jehad Saleh[a]

[a]*Chemical Engineering Department, King Saud University, P.O. Box 800, Riyadh 11421, Saudi Arabia, emails: amkamal@ksu.edu.sa (E. Ali), jsaleh@ksu.edu.sa (J. Saleh)*
[b]*Mechanical Engineering Department, King Saud University, P.O. Box 800, Riyadh 11421, Saudi Arabia, emails: orfij@ksu.edu.sa (J. Orfi), anmohammed@ksu.edu.sa (A. Najib)*

Received 23 June 2018; Accepted 20 November 2018

ABSTRACT

Membrane distillation (MD) uses thermal energy to purify brackish and seawater. The MD-required specific energy is almost ten folds of that required by the conventional thermal and membrane desalination processes. Herein, the performance of the direct-contact membrane distillation (DCMD) unit for the desalination of brackish water was empirically evaluated. The recovery ratio and the thermal efficiency of the unit were found to be very low compared with conventional desalination processes. Different configurations designed to maximize the process performance were thus proposed and investigated theoretically. The investigation involved simulations using a validated DCMD model. The configuration based on permeate-heat recovery offered the maximal gain output ratio (GOR) of up to five when an MD system with a large surface area of 10 m^2 was used. On the other hand, the configuration based on brine recycling outperformed that based on permeate recovery when the surface area of the MD system was less than 6 m^2. Although the cascade configuration with permeate recovery produced the highest GOR, this design suffers from a greater specific capital investment due to the larger number of MD units.

Keywords: Water desalination; Membrane distillation; Brine recycling; Multistage; Energy efficiency

1. Introduction

Membrane distillation (MD) is a hybrid membrane-thermal desalination process for which the driving force is the difference in temperature on the two sides of a hydrophobic membrane. MD offers the advantages of requiring low temperature and pressure levels and affording high rejection rates for nonvolatile components and, therefore, high product quality. MD can be driven by low-grade energy sources such as solar, geothermal, and waste heat sources. However, its performance remains unsatisfactory due to limitations associated with its very low production rate per unit membrane area and its high specific energy consumption. For example, the MD recovery ratio is known to be low, less than 10%. Therefore, improving the performance of the MD system is essential for its expansion and adoption as a reliable desalination process.

Several experimental and theoretical investigations have been conducted to develop methods and evaluate concepts for enhancing the performance of MD systems. Alklaibi and Lior, Matsuura and Khayet, and Camacho et al. [1–3] among others reviewed the status of the MD process and proposed approaches for improvements. Recently, Thomas et al. [4] reported revived attention during the last few decades.

Several concepts and methods have been used to enhance the efficiency of the MD process by improving the recovery ratio and the product flux. In fact, the permeate and brine streams often contain significant amounts of heat that should be recovered and reused to produce more fresh water. Brine

* Corresponding author.

recycling and use of energy recovery devices and hybrid desalination processes are examples of such methods. Other efforts have been made to fulfill the general objective of enhancing the efficiency of the MD process. These attempts and others can be categorized as follows:

- Development of new types of MD membranes specifically targeting fouling, increasing the transported vapor flux and extending the membrane life [3–8].
- Incorporating heat recovery systems into the brine and permeate sides and recycling the brine [9–11]. Several recent studies have focused on reusing the supplied heat via multistage and multiple effect concepts [12–17].
- Use of low cost, renewable energy, and waste heat sources to reduce the overall energy consumption. The appropriate integration of MD units with renewable energy sources is very attractive [4,18–20].
- Developing various configurations for enhancing the efficiency of the MD process, namely, direct contact (DC), air gap, vacuum, and sweeping gas MD. Hence, the development of water gap and material gap MD (21–23), adding spacers in the hot feed path to promote turbulence [24], and the use of a novel coated membrane in hollow-fiber crossflow module for water delamination [25] are examples of this approach.
- Integration of MD with conventional and nonconventional desalination systems is an approach that seems to have a very good impact on increasing the recovery ratio and reducing the specific energy consumption [2,26].
- Advanced theoretical investigations on transport phenomena within the membrane. For example, Eleiwi et al. [27] studied the dynamic modeling of a direct- contact membrane distillation (DCMD) module.

The present study focuses on proposing and assessing configurations with the aim to achieve better energy management within the MD unit. These configurations are essentially based on recovering the heat contained in the permeate and brine and using the multistage structure. Energy and exergy analyses are implemented based on a validated model. The next section of the paper presents a brief description of the experimental setup used to generate important results showing the low performance of such an MD configuration. A model validation is also provided using the experimental results. Section 3 deals with the description of various MD configurations with heat recovery and staging options. The results expressed in terms of variations of recovery ratio, thermal efficiency, exergy destruction, and membrane cost are then presented and discussed.

2. Experimental results and model validation

Fig. 1 illustrates the flow diagram of the MD pilot plant constructed by SolarSpring, Germany. The unit is equipped

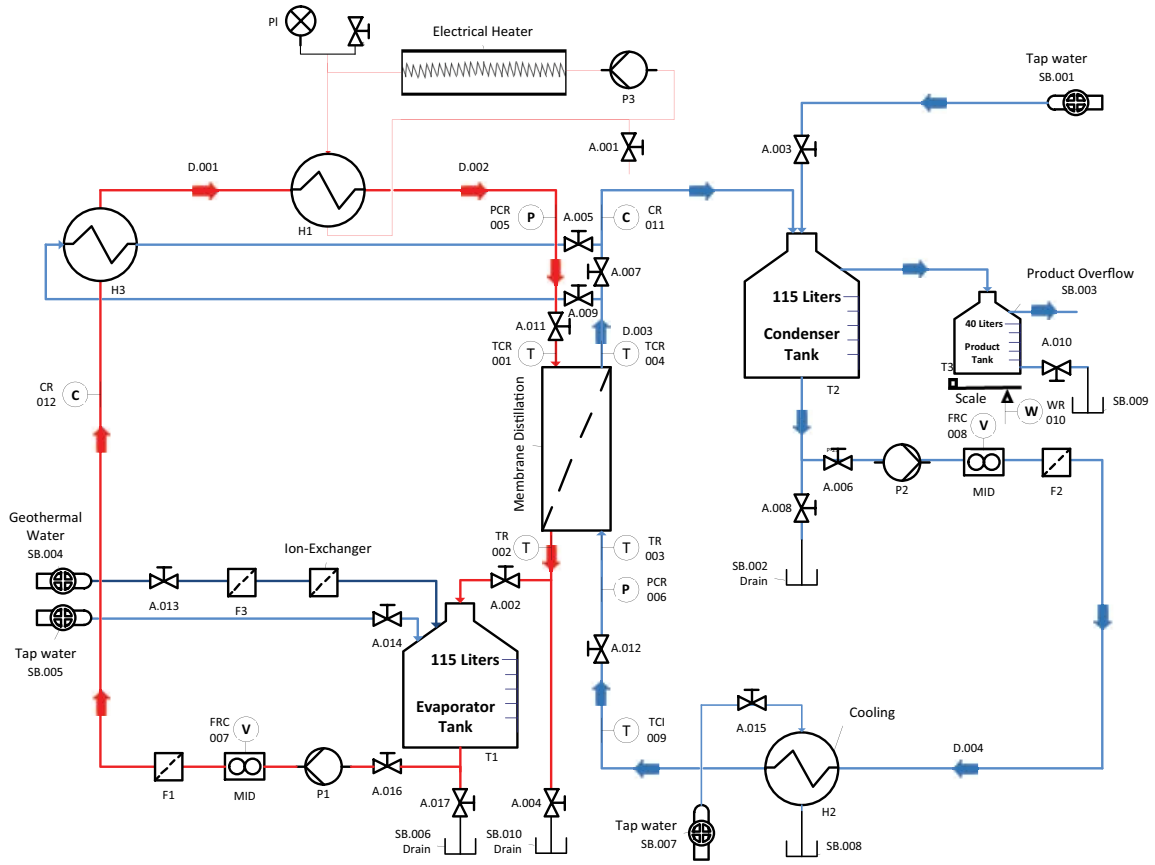

Fig. 1. Schematic of MD pilot plan.

with a DCMD module comprising a 10 m² effective membrane area, 14 m channel length, and 0.7 m channel height. The membrane is 230 μm in thickness with 0.2 μm pore diameter and 2 mm channel gap. DCMD is the simplest and easiest to realize practically and widely employed MD configuration where the permeate water used generally as cooling water is in DC with the membrane surface at the cold side. More details on this MD configuration can be found in refs. [1–3].

The process employs two major water loops. In the brackish water loop, also known as the evaporator loop, brine is withdrawn from storage tank T1, heated in an electrical heater (H1), and pumped through the hot side of the MD unit. The brine leaves the hot side at a lower temperature and returns to T1.

In the condenser loop, raw water is withdrawn from tank T2, cooled to the desired temperature via the heat exchanger (H2) using tap water, and pumped through the cold side of the MD unit. The warm water exiting the condenser loop is recycled to T2. Due to the vapor pressure difference induced by the temperature difference, water evaporates from the hot side and condenses at the cold side as pure water. The distillate is collected as overflow in tank (T3) where it is quantified using an electronic balance. The process employs various sensors to measure the temperature of the four streams around the MD unit, the inlet pressure, and the inlet salinity. The system is also linked to a data acquisition system for data logging and storage.

The pilot plant is employed for desalinating geothermal water taken from a local well. The well temperature is 70°C, and its salinity is 1.414 kg m^{-3}. The present experiment was performed such that the inlet temperature of the hot side was 70°C to simulate the realistic geothermal source. The inlet temperature of the condenser loop was maintained at 25°C. The experimental results are depicted in Fig. 2.

Fig. (2) shows the measured exit temperature of the cold and hot streams and the water mass flux at different feed flow rates. Note that equal flow rates were used for the cold and hot streams. The error bars indicate the measurement uncertainty. Note that error bars will be omitted from the following figures for better visibility. The exit permeate temperature increases with the flow rate until it reaches an asymptotic value. The increase in the permeate temperature is due to enhanced heat transfer induced by increasing turbulence and due to reduced relative heat loss to the surroundings. The exit permeate temperature becomes saturated at higher flow rates because of the limitation imposed by heat losses due to conduction. On another side, Fig. 2 shows the effect of the flow rate on the recovery ratio and gain output ratio (GOR) calculated using Eqs. (A.17) and (A.18). The figure demonstrates that even though the mass flux increases with the flow rate, the recovery ratio does not exceed a maximum value of 5%. The thermal efficiency also remains low.

The experimental data were used to validate the MD model described in Appendix A. Fig. 2 illustrates that the

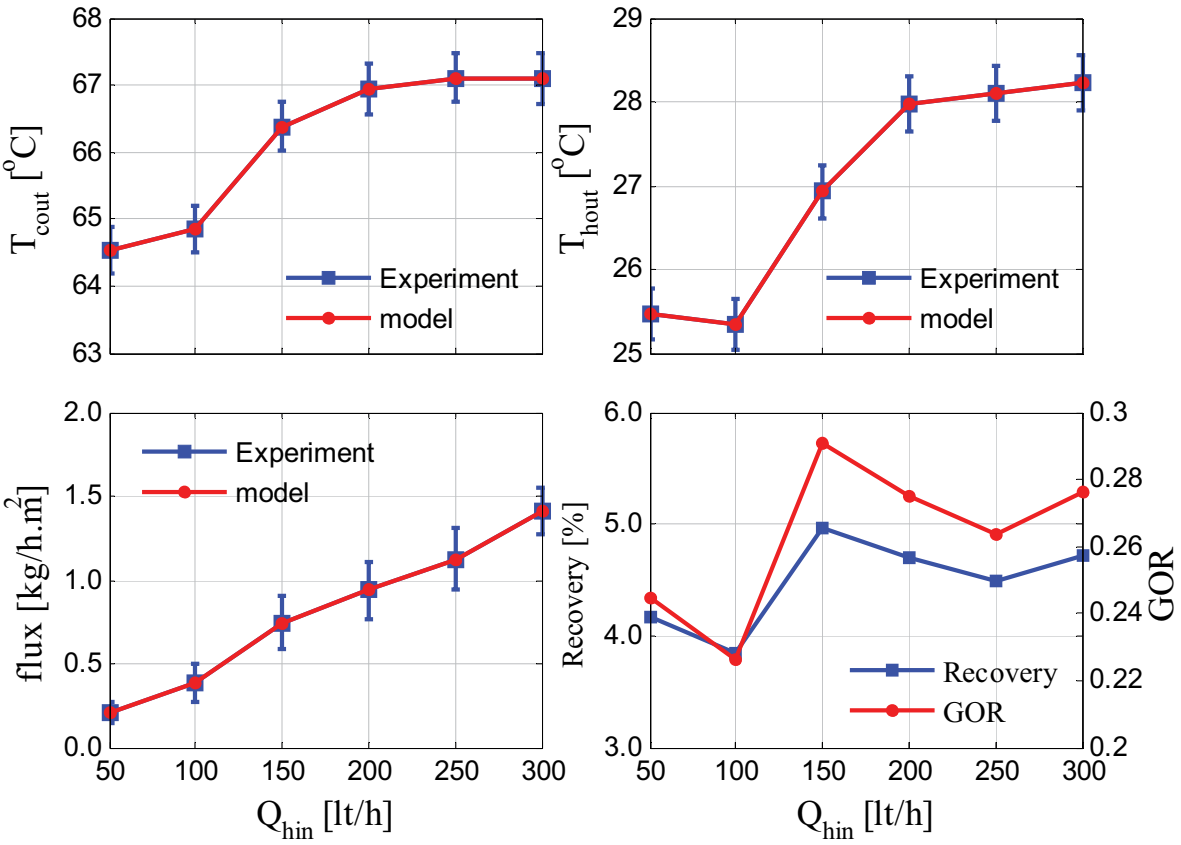

Fig. 2. MD experimental results using real brackish water, inlet feed temperature $T_{h_{out}}$ = 70°C, cooling temperature $T_{c_{in}}$ = 25°C, and inlet feed concentration C_{sf} = 1.4 kg m^{-3}.

model prediction was consistent with the experimental results. The model prediction was improved by adjusting the heat losses to the surroundings to fit experimental data. Further discussion of the process behavior and the model prediction, which is beyond the scope of the present work, can be found elsewhere. Therefore, further details on the experimental results and model validation are provided in refs. [28,29]. The main idea of the inclusion of Fig. 2 is to prove that the model to be used for analyzing the heat and mass transfer in different MD configurations is validated and hence trustworthy.

Notably, several authors have obtained similar low efficiency of the MD process [4,20,30]. This work proposes a theoretical investigation using an experimentally validated model to assess scenarios for achieving better thermal management and thus higher thermal efficiency of the process. Various configurations based on recovering and reusing thermal energy at the permeate and brine exits and expanding the membrane surface area by multistaging are presented and evaluated. The effects of important parameters on the energy use and efficiency of the process are also investigated.

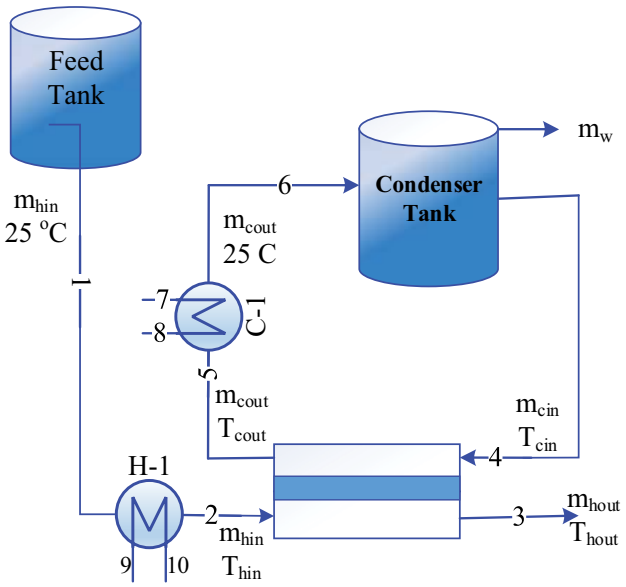

Fig. 3. Baseline design structure.

3. Design structure and methodology

Because the MD operation is based on phase change, i.e., evaporation and condensation, it requires sensible energy for heating and cooling. Depending on the adopted method, the thermal efficiency of the MD process can be quantified using the ratio given in Eq. (A.18), which relates the energy consumed for vaporization to the input heat. Therefore, the higher this ratio, the more efficient the process. This ratio essentially expresses the amount of fresh water produced per unit heat input, as the latent heat of vaporization does not change significantly over the range of operating temperatures. In this case, we use this key performance index (KPI) to compare the process design modifications. Table 1 describes the six considered options giving various heat recovering possibilities. These structures (options) are based on the configurations proposed in the literature to reduce the energy consumption such as permeate-heat recovery, brine recirculation, and multistrand. Note that option 3 is a combination of brine recycling and preheater heat recovery. Similarly, option 6 is a combination of multistage and heat recovery. Hence, the energy efficiency of these different possibilities is compared using the same basis for operating conditions and design parameters. The default structure for water desalination using MD is depicted in Fig. 3, and this default is also denoted as the baseline. This structure is characterized by the absence of any recovery device.

This standard structure uses external heat energy to warm the feed to the desired temperature when non-geothermal water is purified. Alternatively, Fig. 4 shows the MD process with heat recovery [3], which is termed the permeate recovery option herein because thermal energy is recovered from the exiting warm permeate. In this configuration, the permeate stream absorbs the distillate product; therefore, the product is separated and only permeate feed flow is recycled, i.e. $m_{h_{in}} = m_{c_{in}}$. Note that the brine leaving the MD unit is less than the feed. In this case, the feed tank is compensated for this loss from a large reservoir.

The permeate recovery option is particularly applicable to MD with a large heat transfer area that allows for considerable heat transfer from the hot side to the permeate side. On the other hand, when the heat transfer area for MD is insufficient, the brine stream exits at a higher temperature. Therefore, the brine recycling or brine recovery option [31] is recommended, as illustrated in Fig. 5. The configuration shown in Fig. 6 integrates brine and permeate recovery into one system. This might be useful when both the brine and permeates are leaving the MD with significant thermal energy depending on the surface area of the designated MD unit.

Table 1
Summary of the studied MD configurations with heat recovery and staging options

Option number	Option 0 (baseline) configuration	Option 1	Option 2	Option 3	Option 4	Option 5
Description	Single-stage MD with an external heat and cooler	Single-stage MD with permeate-heat recovery	Single-stage MD with brine recovery	Single-stage MD with both permeate and brine recovery	Staged MD in series with brine recovery	Staged MD in series with permeate recovery
Related figures	Fig. 3	Fig. 4	Fig. 5	Fig. 6	Fig. 7	Fig. 8

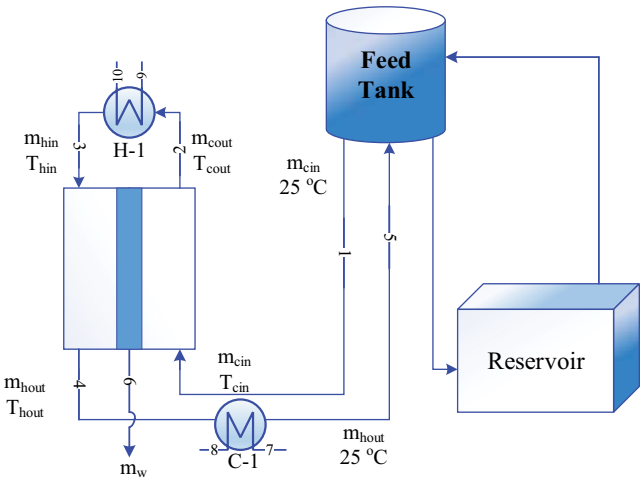

Fig. 4. Design structure for option 1 (a single stage with permeate recovery).

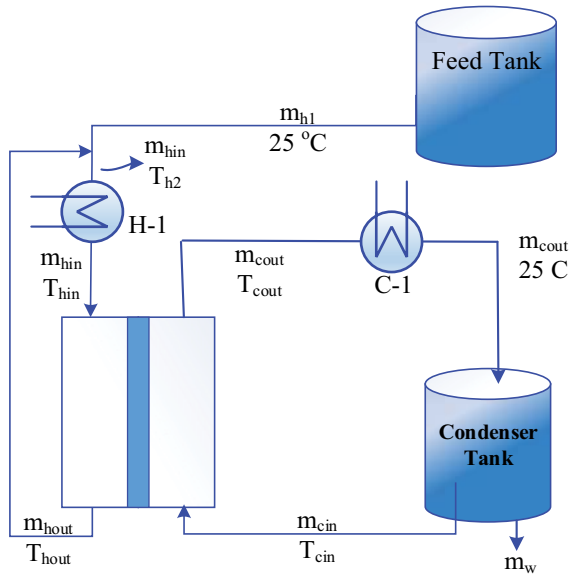

Fig. 5. Design structure for option 2 (1 single-stage MD with brine-heat recovery).

Depending on the relative temperature of the brine and departing permeate, the dotted line in Fig. 6 can be switched between heat exchanger Hx1 and heat exchanger Hx2. For example, if $T_{c_{out}}$ is higher than $T_{h_{out}}$, the dotted line passes through Hx1 first and then Hx2 and vice versa.

Fig. 7 demonstrates the cascaded or staged MD in series [32]. The staged structure facilitates recovery of the thermal energy of the brine by vaporizing an additional amount of water in a subsequent MD stage, as long as the driving force is sufficient. The driving force is simply the temperature difference between the brine and the cold feed permeate. Fig. 7 shows three stages in series for illustration purposes; however, the possible number of stages is determined by the driving force, as discussed further in section 5.1. Fig. 8 is a modification of option 5 that includes heat recovery from the permeate. All stages in options 4 and 5

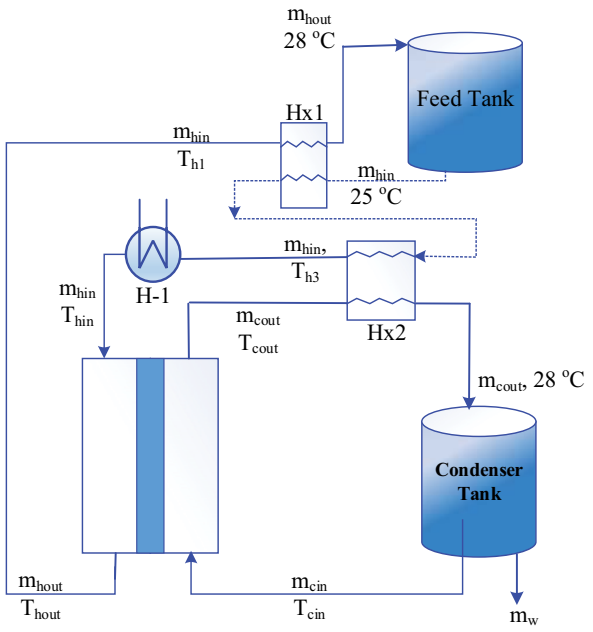

Fig. 6. Design structure for option 3 (a single stage with both brine and permeate recoveries).

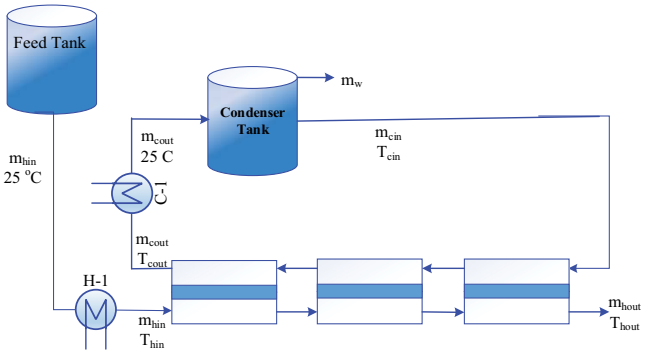

Fig. 7. Design structure for option 4 (multistage structure).

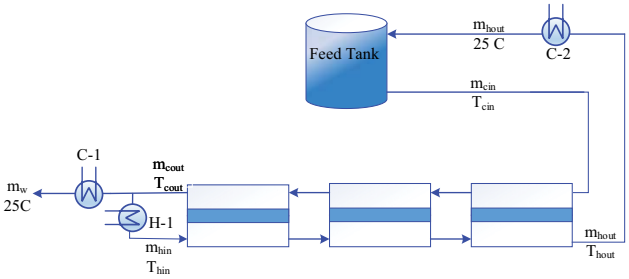

Fig. 8. Design structure for option 5 (multistage structure with brine recirculation).

have the same surface area. Conceptually, staging is similar to increasing the surface area of the MD unit. In this case, the heat recovered from the brine stream is transferred to the permeate stream, causing the permeate to leave the last stage at a higher temperature. Hence, it is of interest to recover the heat from the permeate.

It should be noted that the thermal efficiency will be improved in options 1–3 due to the reduction of the energy load required to preheat the feed in H-1. In option 4, the thermal efficiency is enhanced by increasing water vaporization via cascading. On the other hand, option 5 increases the thermal efficiency by both reducing the heat load of H-1 and increasing water vaporization. Hence, option 5 is expected to deliver the best performance. All of the aforementioned configurations are compared herein using the model developed for the experimental MD rig. A description of the model is presented in Appendix A, and the solution algorithm has been documented by Ali [32]. For a fair comparison, unified MD specifications and operating conditions are used. The operating conditions are as follows: feed flow rate: 300 kg h^{-1}, hot feed temperature: 80°C, cold feed temperature: 25°C, and feed salinity: 1.4 kg m^{-3}. The intermediate variables such as T_{h_2} for option 2 and T_{h_1} and T_{h_3} for option 3 are determined by simple heat balance for each case. Furthermore, the recovery ratio defined by Eq. (A.17) is based on a single pass such that the recovery ratio is unified for all configurations. For entire upcoming simulations, the maximum allowable total surface area for the process is 10 m^2. The total surface area is defined as the area of a single MD unit multiplied by the number of stages. For example, for one stage, the maximum allowed single MD area is 10 m^2; for two stages, the maximum allowed single MD area is 5 m^2; etc. Moreover, the size of single MD and numeric of stages are integer variables. Furthermore, equal single MD size is enforced for all stages. Similarly, for a fair comparison, the maximum allowable $T_{h_{out}}$ is 30°C for all simulations.

4. Exergy analysis principles

Exergy analysis is based on the second law of thermodynamics. Generally, it is used to identify the causes, origins, and magnitudes of process inefficiencies. Exergy is known as the maximum potential work in a system as it interacts with the environment, i.e., the available work lost due to irreversibility. The exergy destruction is an engineering tool for the efficient design of energy-driven systems. The total exergy of the MD process system considered in this study is the sum of the exergy loss in each individual component. For all configurations considered here, the individual components are the MD unit, the primary heater (H-1), the primary cooler (C-1), and the additional heat exchangers utilized in the option 3 configuration. The exergy destruction rate of a control volume at steady state for each component of the system is defined by Kotas [33] as follows:

$$\dot{E}_{\mathrm{xd}} = \sum_{\mathrm{in}} \dot{m}\psi - \sum_{\mathrm{out}} \dot{m}\psi + \sum\left(1+\frac{T_o}{T_k}\right)Q_k - \dot{W} \tag{1}$$

where $\dot{E}_{\mathrm{xd}}$, ψ, $\dot{m}$, and T are the rate of exergy destruction, exergy flow per unit mass, mass flow rate, and temperature, respectively. The subscript o denotes the property value under the surrounding conditions, and the subscript k indicates the property value at state k. The first term on the right-hand side of Eq. (1) is the sum of the exergy input to a controlled volume. The second term is the sum of the exergy output from the controlled volume. The third term represents the exergy of heat Q transferred to the system at constant temperature T. The last term is the mechanical work transfer to or from the system. Neglecting the kinetic and potential exergy, the physical flow exergy per unit mass for a pure substance is defined as follows [33]:

$$\psi = \left(h - h_o\right) - T_o\left(s - s_o\right) \tag{2}$$

where h and s are the specific enthalpy and entropy, respectively, whereas the terms h_o and s_o are the enthalpy and entropy values of the fluid at the reference temperature T_o. The dead-state temperature and pressure are taken as 20°C and 101.325 kPa, respectively. The effect of the salinity is ignored. In this study, the total exergy loss is used as a performance index to compare the effectiveness of the proposed configurations.

5. Results and discussion

The surface area of the MD unit has an important impact on the overall mass and heat transfer through the membrane interface. Hence, it is an effective factor influencing the MD performance. Moreover, it affects the process economics as the membrane capital cost is proportional to the surface area. Consequently, we compare the thermal effectiveness of the proposed design configuration over a selected range of values for the surface area. Note, the experimental original MD setup has a surface area of 10 m^2, but we examine the performance at other surface area values via simulation using the validated model.

5.1. Recovery ratio and thermal efficiency

Fig. 9 compares the performance of the MD systems in terms of the recovery ratio and thermal efficiency for the six configurations (options). The definition of recovery ratio and thermal efficiency GOR is given by Eqs. (A.17)–(A.19).

In addition, Fig. 9(a) and (b) illustrates how the temperatures of the departing streams ($T_{c_{out}}$ and $T_{h_{out}}$, i.e. the exit permeate and brine temperatures, respectively) change with the surface area of the MD unit. The profiles of these temperatures are presented and discussed because they are strongly related to the recovery ratio and thermal efficiency. For a small surface area, the permeate and brine streams both exit at almost the same moderate temperature. When the area increases, the overall heat transfer from the hot side to the cold side increases accordingly, causing the permeate temperature to increase considerably to a maximum of 75°C and the brine temperature to drop to a minimum of 29°C. This variation in the temperature with the area will affect the thermal efficiency of the different process configurations. Furthermore, this variation was common to all cases except options 4 and 5. The temperature profile for the latter cases is discussed in section 5.1. The identical temperature profile of options 1–3 and the baseline is reasonable because a single MD unit was used and the same operating conditions were enforced in all cases.

For the same reasons mentioned above, a unique recovery ratio was obtained for these cases, as depicted in Fig. 9(c). Options 4 and 5 are exceptions, where their corresponding recovery ratios are identical and remain almost close to 5.5%. The recovery ratios for options 4 and 5 differ than the other

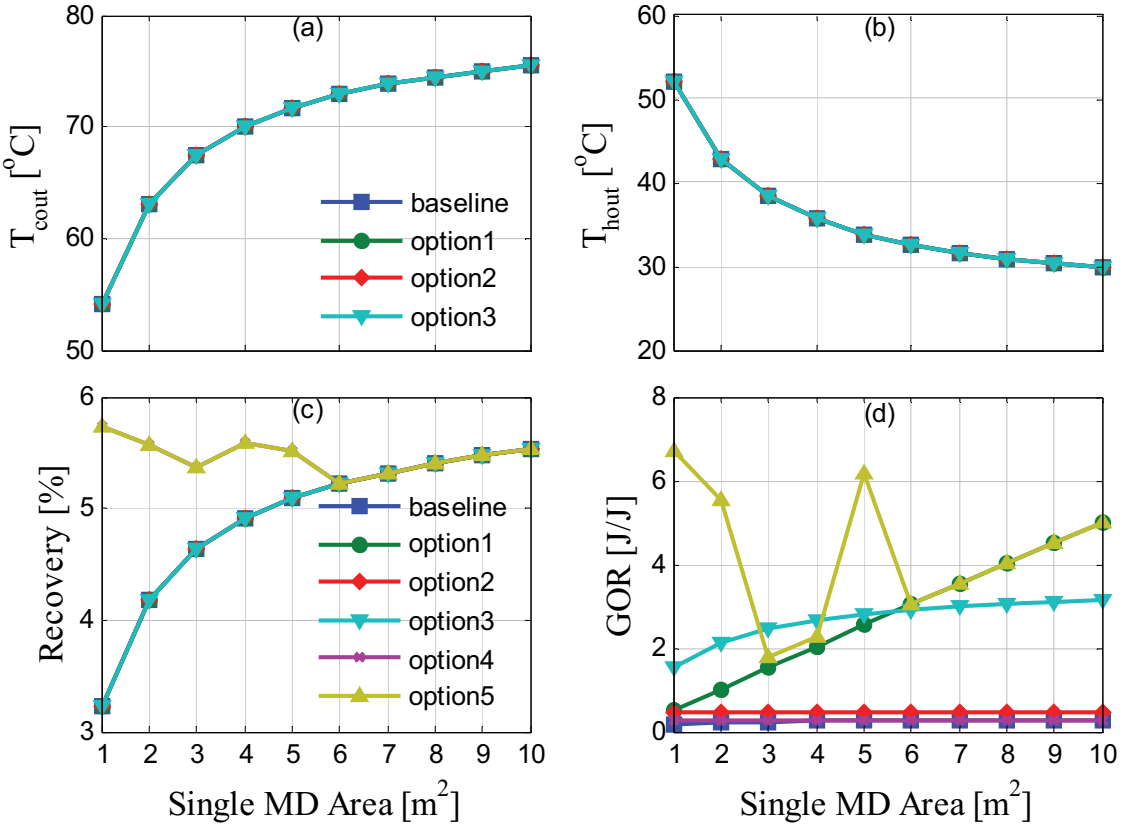

Fig. 9. Comparison of the MD performance of different configurations (a) Tcout, (b) Thout, (c) Recovery ratio, and (d) GOR.

cases at surface area lower than 6 m^2 but become identical afterward.

However, the GOR was dissimilar for all proposed configurations, as shown in Fig. 9(d). In fact, the baseline, option 2, and option 4 had the lowest GOR, whereas option 1, option 3, and option 5 had unique thermal efficiencies. For option 1, the GOR increased linearly with the area because $T_{c_{out}}$ increased considerably, as mentioned earlier, leading to a remarkable reduction in the heat duty of the feed preheater (H-1). Option 3 showed a slow and monotonous improvement in the thermal efficiency because the heat recovered from the reject brine and outlet permeate is limited by the thermodynamic efficiency of the heat exchangers Hx1 and Hx2. Interestingly, for a small surface area, i.e., less than 6 m^2, the hybrid heat recovery (option 3) was superior to the permeate recovery (option1) in terms of providing a higher GOR. In comparison, for a surface area larger than 6 m^2, option 1 provided superior performance. In fact, option 1 furnished a high GOR of five for a surface area of 10 m^2. Option 5 delivered an irregular response over the range of surface areas because the production rate is a function of both the surface area and number of stages. In fact, the number of stages and surface area are interrelated as discussed below in relation to Fig. 10. Nevertheless, option 5 afforded the best performance in terms of the recovery ratio and thermal efficiency over the entire surface area range due to the staged structure.

It should be noted that option 2 had a low GOR because the brine temperature remained lower than that of the permeate over the entire surface area range. Therefore, the contribution of the former to the heating duty of H-1 remained minor.

Fig. 10 demonstrates the performance achieved with options 4 and 5 independent of the other cases due to the distinct results obtained with these options. These two configurations produced irregular responses, i.e. discontinuity, because of the combined effect of the surface area size of single MD and number of stages involved bearing in mind that both of them are integer variables. The results in Fig. 10 are plotted against the size of a single MD unit. As shown in Fig. 10(b), since we are dealing with multistage, for each single MD size, different number of stages are used to achieve a brine temperature of ≤30°C at the last stage, which is the temperature obtained when a single 10-m^2 MD unit is used. The required number of stages for each single MD size was determined by sequential iteration. For instance, for a given surface area, the model for a single MD is solved if $T_{h_{out}} \leq 30$°C iteration stops. Otherwise, a train of two stages is tried and so on. For example, Fig. 10(b) shows that eight stages are needed when an MD unit with a surface area of 1 m^2 is used, which makes the total surface area equal to 8 m^2. For MD with an area of 6 m^2 and higher, a single stage is sufficient. In fact, for a single MD size of 6 m^2 and higher, only one stage can be employed because the total surface area is limited to 10 m^2. Nevertheless, it turned out that one stage of single MD size of 6–10 m^2 was sufficient to make $T_{h_{out}}$ equal to 30°C. Notably, because the number of stages is an integer variable and an equally fixed integer MD size is used for all stages, nonlinearity is induced in the numerical solution of the model.

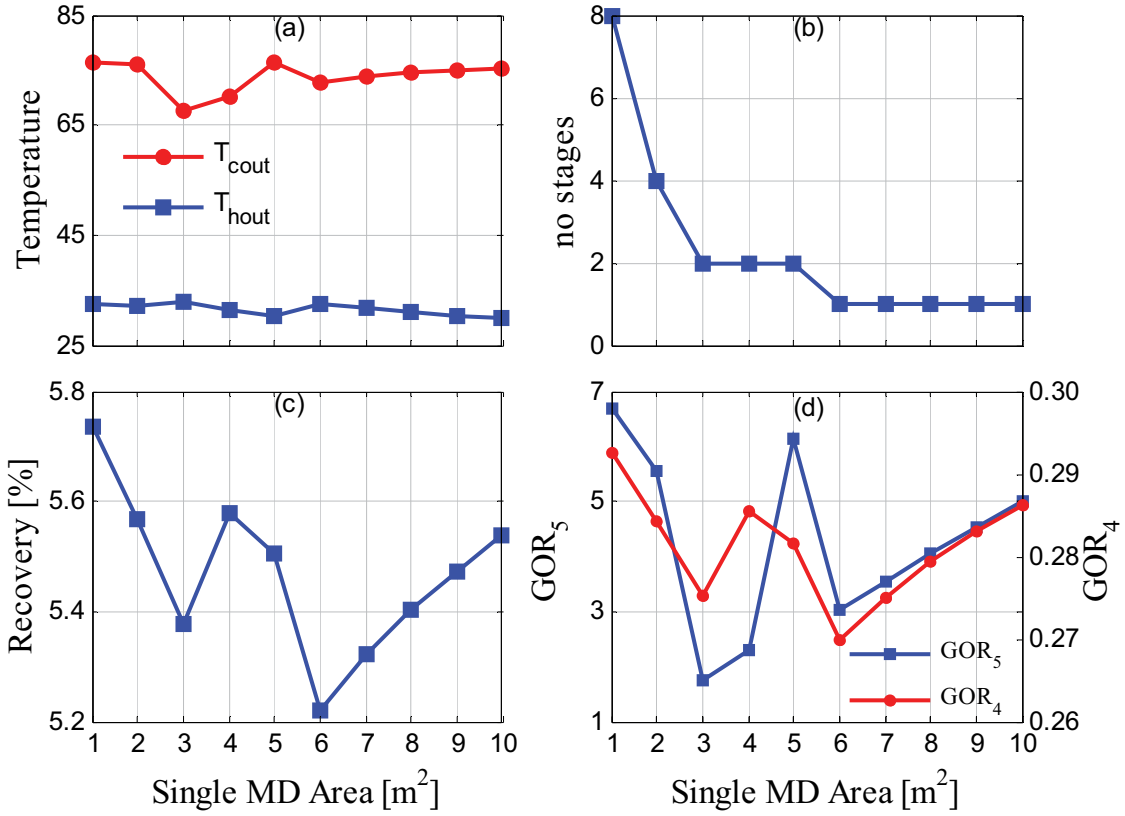

Fig. 10. Performance of options 4 and 5 vs. surface area (a) Temperature, (b) number of stages, (c) Recovery ratio, and (d) GOR.

This nonlinearity creates fluctuation in $T_{c_{out}}$ and consequently in the mass flux. Because staging is conceptually similar to increasing the surface area, the temperature of the brine and permeate should reach their extreme values when the total surface area is large. Hence, the brine temperature remained around 30°C and the permeate temperature around 75°C. Some fluctuations in $T_{c_{out}}$ were observed for surface areas in the range of 3–6 m² although the number of stages used was the same, e.g., two stages. Note that although the number of stages was constant in these cases, i.e. 2, the total surface area was different because the size of the individual MD units is dissimilar. This variation affects the calculation of $T_{c_{out}}$ and consequently the recovery rate, as shown in Fig. 10(c). Moreover, because the number of stages is an integer variable and a fixed membrane size is used for all stages for a given MD surface area, nonlinearity is induced in the numerical solution of the model. As shown in Fig. 10(c), despite the minor variation in the recovery rate with the surface area, a recovery rate of around 5% (5.2%–5.7%) was obtained over the entire surface area range. According to Eq. (A.17), the recovery rate is proportional to the mass production which is a multiplication of mass flux by the surface area. For small surface areas, e.g. less than 6 m², the mass production is small. At surface area equal to and larger than 6 m², the mass flux is higher. However, the number of stages involved in both cases is different which makes the overall recovery rate almost the same around 5%. Note that the temperature and recovery rate profiles for options 4 and 5 were exactly similar because these parameters are not affected by the heat recovery of the permeate stream. The GOR for option 4 followed the same trend as the recovery ratio because like the recovery ratio, the GOR is proportional to the production rate given that the heat input is constant. On the other hand, the GOR for option 5 was affected by both the production rate and heat input as the latter varies with $T_{c_{out}}$ according to Eq. (A.19). As a result, the GOR for option 5 was much larger than that of option 4 and followed a slightly different trend with variation of the surface area. For example, GOR_5 (where the subscript indicates the option) increased at 5 m², whereas GOR_4 decreased, although the production rate declined at that specific area, as manifested by the recovery ratio. The steep increase in GOR_5 is due to the increase in $T_{c_{out}}$ between 4 and 5 m². Fig. 10(b) shows that for MD sizes of 6 m² and above, only one stage is required. Moreover, the recovery ratio and the GOR between 6 and 10 m² were identical to those of option 1 (Fig. 9(d)) because in both cases, only one stage was employed. It should be noted that our finding for options 4 and 5 which use the multistage concept is consistent with that of Lee et al. [17]. They reported a GOR less than 1 for a cascade of 4 and 8 DCMD stages when no heat recovery is involved. However, when heat recovery is involved, the GOR becomes larger than 2 when 4 stages are used and around 8 when 8 stages are used. In addition, our observation regarding the relationship between the number of stages and surface area (Fig. 9(b)) is also in agreement with that reported by Ali et al. [34]. They have shown that the number of required stages to achieve 70% recovery factor decreases with area per stage. In our case, we have fixed $T_{h_{out}}$ instead of the recovery factor bearing

in mind that the former is related indirectly to the recovery ratio. In general, keeping the temperature drop as large as possible by fixing $T_{h_{out}}$ will improve the thermal efficiency of the system and hence fixes the overall recovery ratio because all other operation conditions are constant.

5.2. Exergy analysis

The exergy flow for each stream of the baseline option is listed in Table 2. Cold water (20°C) was used in the cooler (C-1) and saturated steam at 100°C and 1 bar was used in the preheater (H-1). The corresponding mass flow rates were computed by simple heat balance around each unit. The data in Table 2 were used to calculate the exergy losses for each component, as listed in Table 3. The baseline had a total exergy destruction of 5 kW when an MD system with a surface area of 1 m² was used. This total exergy destruction rate represents about 58% of the total exergy entering the unit. Similar results were obtained with different MD unit sizes. Using the same approach, the exergy losses for the other options with different surface areas could be obtained.

Fig. 11 compares the overall exergy destruction for all options as a function of the membrane area. The baseline and option 4 had the largest exergy losses among the configurations.

Option 2 had a smaller exergy loss when the membrane area was 1 m², but the exergy loss increased monotonically as the membrane surface area increased. As previously found, options 1, 3, and 5 delivered the best performance of the various options. These configurations provided the least irreversibility due to a considerable reduction of the heat energy consumed by H1, bearing in mind that the exergy losses of H1 were greater than those of the other units in the process. Reduction of the heat duty in H1 in these cases was achieved by recovering the heat energy from the permeate. For the largest membrane surface area, options 1 and 3 had the lowest exergy losses (less than 0.5 kW) because as discussed earlier, the heat recovery is more efficient when the MD system size is large. Distinguishingly, option 5 had the smallest exergy destruction for a membrane size of 1 m². However, at this MD system size, eight stages were used, which makes the overall equivalent surface area equal to 8 m². This enlarged surface area due to cascading caused the permeate-heat recovery for option 5 to be superior to that of options 1 and 3, resulting in less irreversibility for the former. Based on the data in Figs. 10 and 11, configuration option 1 delivered the largest GOR and lowest exergy losses when a 10-m² MD system was used. Similarly, option 5 furnished the highest GOR and the least exergy destruction when eight stages each with a 1-m² surface area were utilized. In both cases, the enhanced performance was achieved at the expense of greater capital cost. The capital investment is proportional to the MD surface area and to the number of MD units.

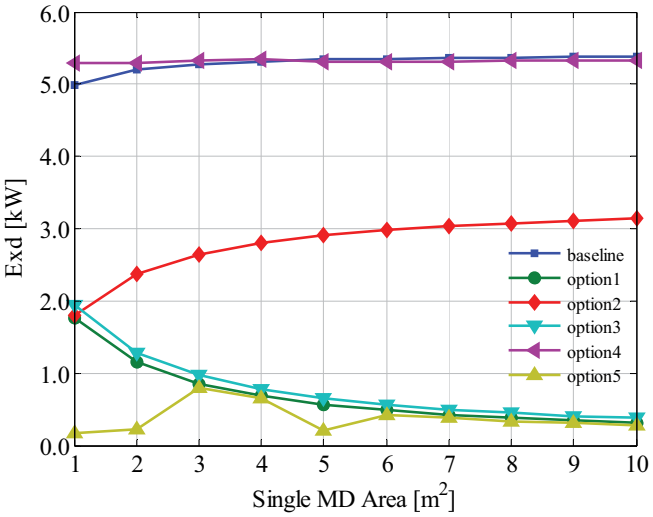

Fig. 11. Variation of the exergy destruction for each option with the membrane area.

Table 2
Exergy flow for baseline case at A = 1 m²

Stream	T	h	s	m	$\dot{E}_x$
	K	kJ kg^{-1}	kJ kg^{-1} K	kg s^{-1}	kJ s^{-1}
1	298	18.95	0.06	0.09	0.01
2	353	229.46	0.71	0.09	1.78
3	298	20.93	0.07	0.09	0.02
4	325	121.75	0.39	0.08	0.52
5	327	142.92	0.46	0.09	0.66
6	298	20.93	0.07	0.09	0.02
7	293	0.00	0.00	0.26	0.00
8	303	41.84	0.14	0.26	0.18
9	373	2,675.70	7.35	0.01	6.11
10	373	419.10	1.31	0.01	0.46

Table 3
Exergy losses for baseline case at A = 1 m²

Component	Exergy in (kW)	Exergy out (kW)	Exergy loss (kW)
MD	1.79	1.18	0.61
C-1	0.66	0.20	0.47
H-1	6.12	2.24	3.88
Total	8.58	3.62	4.96

5.3. Effect of surface area

It is obvious from the above results that the surface area has a great impact on the system performance. In particular, the MD system with a surface area of 6 m² exhibited some special characteristics. For example, the GOR of options 1 and 3 intersected at that surface area. In addition, for options 4 and 5, one stage of 6 m² was sufficient for performing the MD process with the maximum possible heat transfer. The higher recovery ratio obtained beyond 6 m² was due to the increased unit capacity. Fig. 9 shows that $T_{c_{out}}$ increased rapidly at small surface areas but asymptotically at large surface areas. Our simulations revealed that as the surface area increased beyond 10 m², $T_{c_{out}}$ increased marginally as it cannot approach the hot feed temperature due to the thermodynamic limitation imposed by heat losses due to conduction in the membrane

material and/or convection to the surroundings. Moreover, the capital cost of the membrane increases with the unit size. Therefore, increasing the MD surface area is not economical.

The following literature procedure was used to evaluate the effect of the surface area on the specific capital cost for the various options [35]:

The annualized capital investment can be estimated from Eq. (3):

$$\mathrm{ACC}\left(\frac{\$}{y}\right)=\mathrm{TC}\frac{i(i+1)^n}{(i+1)^n-1} \tag{3}$$

where i is the interest rate taken as 10% and n is the number of years taken as 10 years. The total capital cost is related to the equipment cost according to the equation:

$$\mathrm{TC}=1.65\mathrm{EC} \tag{4}$$

Generally, the equipment cost includes the cost of heat exchangers, pumps, etc. However, we limit our analysis to the cost of the membrane unit:

$$\mathrm{EC}=C_{\mathrm{mem}}A \tag{5}$$

where A is the surface area in m^2 and C_{mem} is the membrane cost, which ranges between 30 and 100 \$ m^{-2}. In this study, we chose 65 \$ m^{-2}. It should be noted that the total surface area was used in Eq. (5); for example, for options 4 and 5, the sum of the surface area for all stages was used. We normalized the annualized capital investment by the production rate as follows:

$$\mathrm{SPAC}\left(\frac{\$}{m^3}\right)=\frac{\mathrm{ACC}}{m_W\times 24\times 365/\rho} \tag{6}$$

The variation of SPAC with the surface area for all options is shown in Fig. 12.

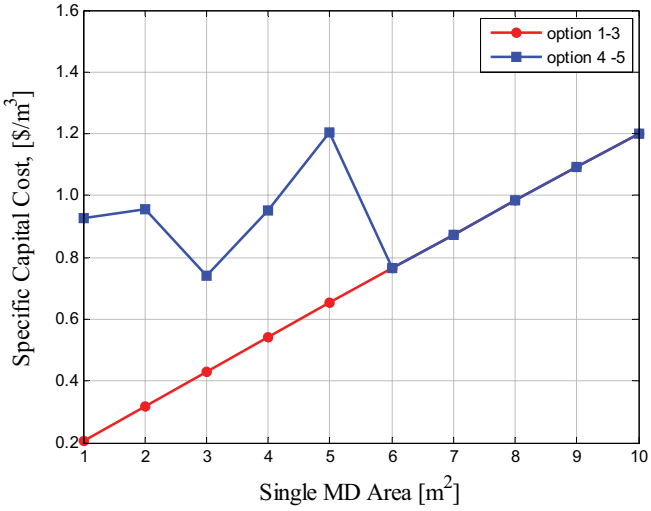

Fig. 12. Specific capital investment versus membrane surface area.

Table 4
Comparison of KPI for all options for surface area range of 1–10 m^2

Option 1	Recovery ratio (%)	GOR (kJ kJ^{-1})	Exergy losses (kW)	Capital cost ([\$ m^{-3})
Baseline	3.2–5.5	0.16–0.28	4.98–5.38	0.2–1.2
Option 1	3.2–5.5	0.5–5.0	1.76–0.31	0.2–1.2
Option 2	3.2–5.5	0.46–0.45	1.8–3.14	0.2–1.2
Option 3	3.2–5.5	1.5–3.2	1.95–0.38	0.2–1.2
Option 4*	5.7–5.5	0.29–0.28	5.29–5.33	0.9–1.2
Option 5*	5.7–5.5	6.7–5.0	0.174–0.284	0.9–1.2

*Terminal values, otherwise KPI may have lower or higher than the terminal values.

It is obvious that the specific capital cost increased linearly with the surface area for options 1–3; therefore, it is preferable to use a small size MD system to minimize the annualized investment. For single-stage options (options 1–3), the unit cost increases at a higher rate with unit size relative to recovery ratio rate. Moreover, options 4 and 5 are inferior to the others, especially when the MD size is less than 6 m^2. In fact, options 4 and 5 incur larger specific capital costs at lower surface areas. This is because the recovery ratio is almost constant over the range of unit size while the unit cost increases rapidly with area per unit. Depending on the operating temperature, Ali et al [34] have also reported increasing specific fixed cost with membrane length for a fixed recovery factor of 70%.

To summarize the comparison of the proposed MD configurations, we list, in Table 4, the KPI values over the range of MD surface area. Three major observations can be drawn from Table 4. First, GOR is the most effective KPI for comparison because it has different influence on each configuration. Second, option 5 seems to outperform other configurations as it has the highest recovery ratio and GOR and lowest exergy losses with reasonable capital cost compared with the other structures. Lastly, increasing the MD surface area beyond 6 m^2 is discreet for performance differentiation as the recovery ratio and specific capital cost become identical for all cases. Moreover, the thermal efficiency becomes either identical for specific cases or invariant for other cases. However, as exergy losses are concerned, increasing the MD surface area can decrease the exergy losses by 70% for options 1, 3, and 5.

6. Conclusions

DCMD is a useful process for the desalination of brackish water. However, DCMD consumes a significant amount of energy for heating and cooling. A mathematical model was validated using experimental data and was used to test the efficacy of different design configurations for enhancing the MD performance. The configurations are based on recovering the thermal energy contained in the permeate and/or brine streams. MD staging in series was also examined. Besides, the analysis of the performance of each configuration is based on the evaluation of the recovery ratio, gained output ratio, exergy destruction rate, and membrane cost.

Membrane surface area was varied in the study from 1 to 10 m^2. The data reveal that permeate-heat recovery (option 1) improves the thermal efficiency of the process if the MD system has a surface area larger than 6 m^2. On the other hand, combined permeate- and brine-heat recovery (option 3) may be more energy efficient than the other cases when the MD surface area is less than 6 m^2. The exception is option 5 which may outperform option 3 when area per MD unit is smaller than 6 m^2. The cascading multi-MD unit configuration is found to deliver the best thermal performance relative to the other configurations for all surface areas where only one permeate-heat recovery step is incorporated. Nevertheless, the cascade configuration demands a larger overall surface area due to the increased number of stages. Hence, additional capital investment is needed.

Acknowledgment

This project was supported by King Saud University, Deanship of Scientific Research, Research Group Grant 1438-093.

Symbols

A_s — MD surface area, m^2
A — MD cross-sectional area, m^2
ACC — Annualized capital cost, \$ y^{-1}
C_m — Permeability coefficient, kg m^{-2} s Pa
C_m^k — Knudsen mass flux coefficient, kg m^{-2} s Pa
C_m^d — Molecular diffusion mass flux coefficient, kg m^{-2} s Pa
C_m^C — Transition mass flux coefficient, kg m^{-2} s Pa
C_s — Salinity of brackish water, kg m^{-3}
Cp — Heat capacity, J kg^{-1} K
C_{mem} — Membrane cost per area, \$ m^{-2}
d_h — Hydraulic diameter of channel in RO unit, m
EC — Equipment cost, \$
GOR — Gained output ratio
H_v — Heat of vaporization, J h^{-1}
H_{in} — Enthalpy of hot feed in MD unit, W
h_f, h_p, h_m — Feed, permeate, and membrane heat transfer coefficient, W m^{-2} K
J — Mass flux in MD module, kg m^{-2} h
k_m — MD membrane conductivity, W m^{-1} K
M_w — Molecular weight of water, g mol^{-1}
$m_{h_{\text{in}}}$, $m_{h_{\text{out}}}$ — Hot water inlet and outlet flow rate, respectively, kg h^{-1}
m_c — Cold water volumetric flow rate, kg h^{-1}
m_w — Permeate and distillate flow rate, respectively, kg h^{-1}
P_f, P_b — feed and brine pressure (bar)
P_1, P_2 — Vapor pressure at feed and permeate membrane surface, Pa
PD — Membrane pressure multiplied by diffusivity, Pa m^2 s^{-1}
P_a — Entrapped air pressure, Pa
q_f, q_p — Heat transfer rate at feed and permeate sections, W m^{-2}
q_m — Heat of evaporation and conduction, W m^{-2}
Q — Overall heat flux, W m^{-2}
Rc — Recovery ratio, %
Re — Reynolds number
r — MD pore size, m
R — Ideal gas constant, J mol^{-1} K
Sc — Schmidt number
Sh — Sherwood number
SPAC — Specific annualized cost, \$ m^{-3}
T, T_0 — Feed water and reference temperature, °C
T_h, T_c — Feed (hot) and permeate (cold) bulk temperature, K
T_{hm}, T_{cm} — Feed and permeate membrane temperature, K
T_{ref} — Reference temperature, K
TC — Total capital cost, \$
u — Velocity of water in feed channel, m h^{-1}
U — Overall heat transfer coefficient, W m^{-2} K

Greek

l — Latent heat of vaporization, J kg^{-1}
e — Termination criteria for algorithms
e_m — MD porosity
n — Kinematic viscosity, m^2 h^{-1}
t — MD membrane tortuosity
d — MD membrane thickness, mm
r — Density, kg m^{-3}

References

[1] A.M. Alklaibi, N. Lior, Membrane-distillation desalination: status and potential, Desalination, 171 (2004) 111–131.
[2] T. Matsuura, M. Khayet, Membrane Distillation: Principles and Applications, Elsevier, Netherland, 2011, p. 477.
[3] L.M. Camacho, L. Dumée, J. Zhang, J.D. Li, M. Duke, J. Gomez, S. Gray, Advances in membrane distillation for water desalination and purification applications, Water, 5 (2013) 94–196.
[4] N. Thomas, M.O. Mavukkandy, S. Loutatidou, H.A. Arafat, Membrane distillation research and implementation: lessons from the past five decades, Sep. Purif. Technol., 189 (2017) 108–127.
[5] M.I. Ali, E.K. Summers, H.A. Arafat, J.H. Lienhard, Effects of membrane properties on water production cost in small scale membrane distillation systems, Desalination, 306 (2012) 60–71.
[6] A. Ali, C. Quist-Jensen, F. Macedonio, E. Drioli, On designing of membrane thickness and thermal conductivity for large scale membrane distillation modules, J. Membr. Sci. Res., 2 (2016) 179–185.
[7] M. Khayet, Membranes and theoretical modeling of membrane distillation: a review, Adv. Colloid Interface Sci., 164 (2011) 56–88.
[8] E. Drioli, A. Ali, F. Macedonio, Membrane distillation: recent developments and perspectives, Desalination, 356 (2015) 56–84.
[9] E. Summers, H.A. Arafat, J.H. Lienhard, Energy efficiency comparison of single-stage membrane distillation (MD) desalination cycles in different configurations, Desalination, 290 (2012) 54–66.
[10] J. Swaminathan, H.W. Chung, D.M. Warsinger, J.H. Lienhard, Energy efficiency of membrane distillation up to high salinity: Evaluating critical system size and optimal membrane thickness, Appl. Energy, 211 (2018) 715–734.
[11] O.R. Lokare, S. Tavakkoli, V. Khanna, R.D. Vidic, Importance of feed recirculation for the overall energy consumption in membrane distillation systems, Desalination, 428 (2018) 250–254.
[12] J.G. Lee, W.S. Kim, J.S. Choi, N. Ghaffour, Y.D. Kim, A novel *multi-stage* direct contact *membrane distillation* module: design, experimental and theoretical approaches, Water Res., 107 (2016) 47–56.
[13] J.G. Lee, A.S. Alsaadi, A.M. Karam, L. Francis, S. Soutane, N. Ghaffour, Total water production capacity inversion phenomenon in multi-stage direct contact membrane distillation: a theoretical study, J. Membr. Sci., 544 (2017) 126–134.

[14] E. Khalifa, S.M. Alawad, M.A. Antar, Parallel and series *multistage air* gap *membrane distillation*, Desalination, 417 (2017) 69–76.
[15] *B.L. Pangarkar, S.K.* Deshmukh, Theoretical and experimental analysis of multi-effect air gap membrane distillation process (ME-AGMD), J. Environ. Chem. Eng., 3 (2015) 2127–2135.
[16] J. Gilron, L. Song, K.K. Sirkar, Design for cascade of crossflow direct contact membrane distillation, Ind. Eng. Chem. Res., 46 (2007) 2324–2334.
[17] H. Lee, F. He, L. Song, J. Gilron, K.K. Sirkar, Desalination with a cascade of cross-flow hollow fiber membrane distillation devices integrated with a heat exchanger, AIChE J., 57 (2011) 1780–1795.
[18] M.R. Qtaishat, F. Banat, Desalination by solar powered membrane distillation systems, Desalination, 308 (2013) 186–197.
[19] F. Banat, N. Jwaied, M. Rommel, J. Koschikowski, M. Wieghaus, Desalination by a "compact SMADES" autonomous solar-powered membrane distillation unit, Desalination, 217 (2007) 29–37.
[20] J.H. Lienhard, M.A. Antar, A. Smith, J. Blanco, G. Zaragoza, Solar desalination, Annu. Rev. Heat Transfer, 15 (2012) 277–347.
[21] E. Khalifa, Water and air gap membrane distillation for water desalination—An experimental comparative study, Sep. Purif. Technol., 141 (2015) 276–284.
[22] L. Francis, N. Ghaffour, A.A. Alsaadi, G.L. Amy, Material gap membrane distillation: a new design for water vapor flux enhancement, J. Membr. Sci., 448 (2013) 240–247.
[23] J. Swaminathan, H.W. Chung, D. Warsinger, F. Al-Marzooqi, H.A. Arafat, J.H. Lienhard, Energy efficiency of permeate gap and novel conductive gap membrane distillation. J. Membr. Sci., 502 (2016) 171–178.
[24] Y. Taamneh, K. Bataineh, Improving the performance of direct contact *membrane distillation* utilizing *spacer*-filled channel, Desalination, 408 (2017) 25–35.
[25] D. Singh, P. Prakash, K.K. Sirkar, Deoiled produced water treatment using direct-contact membrane distillation, Ind. Eng. Chem. Res., 52 (2013) 13439–13448.
[26] J. Orfi, A. Najib, E. Ali, A. Ajbar, M. AlMatrafi, M. Boumaaza, K. Alhumaizi, Membrane distillation and reverse osmosis-based desalination driven by geothermal energy sources, Desal. Wat. Treat., 76 (2017) 40–52.
[27] F. Eleiwi, N. Ghaffour, A.S. Alsaadi, L. Francis, T.M. Laleg-Kirati, Dynamic modeling and experimental validation for direct contact membrane distillation (DCMD) process, Desalination, 384 (2016) 1–11.
[28] E. Ali, J. Orfi, A. Najib, Assessing the thermal efficiency of brackish water desalination by membrane distillation using exergy analysis, Arab. J. Sci. Eng., 43 (2018) 2413–2424.
[29] E. Ali, J. Orfi, An experimentally calibrated model for heat and mass transfer in direct contact membrane distillation, Desal. Wat. Treat., 116 (2018) 1–18.
[30] D. Winter, J. Koschikowski, S. Ripperger, Desalination using membrane distillation: flux enhancement by feed water deaeration on spiral-wound modules, J. Membr. Sci., 423–424 (15) (2012) 215–224.
[31] H.C. Duong, P. Cooper, B. Nelemans, T.Y. Cath, L.D. Nghiem, Optimizing the thermal efficiency of direct contact membrane distillation by brine recycling for small-scale seawater desalination, Desalination, 374 (2015) 1–9.
[32] E. Ali, Energy efficient configuration of membrane distillation units for brackish water desalination using exergy analysis, Chem. Eng. Res. Des., 125 (2017) 245–256.
[33] T.J. Kotas, The Exergy Method of Thermal Plant Analysis, Anchor Brendon, Great Britain, 1985.
[34] A. Ali, C.A. Quist-Jensen, F. Macedonio, E. Drioli, Optimization of module length for continuous direct contact membrane distillation process, Chem. Eng. Process. Process Intensif., 110 (2016) 188–200.
[35] Y.J. Choi, S. Lee, J. Koo, S.H. Kim, Evaluation of economic feasibility of reverse osmosis and membrane distillation hybrid system for desalination, Desal. Wat. Treat., 57 (2016) 24662–24673.
[36] D.J. Lawal, A. Khalifa, Flux prediction in direct contact membrane distillation, Int. J. Mater. Mech. Manuf., 2(4) (2014) 302–308.
[37] K. Fard, Y.M. Manawi, T. Rhadfi, K.A. Mahmoud, M. Khraisheh, F. Benyahia, Synoptic analysis of direct contact membrane distillation performance in Qatar: a case study, Desalination, 360 (2015) 97–107.
[38] J. Zhang, Theoretical and Experimental Investigation of Membrane Distillation, PhD Thesis, Victoria University, Australia, 2011.
[39] M. Safavi, T. Mohammadi, High-salinity water desalination using VMD, Chem. Eng. J., 149 (2009) 191–195.
[40] T.C. Chen, C.D. Ho, Immediate assisted solar direct contact membrane distillation in saline water desalination, J. Membr. Sci., 358 (2010) 122–130.

Appendix A

Direct- contact membrane distillation (DCMD) desalination unit model

The mass flux (J) of vapor transfer through pores is given by

$$J = C_m\left(P_1 - P_2\right)\left(\frac{\text{kg}}{\frac{\text{m}^2}{\text{s}}}\right) \tag{A.1}$$

In Eq. (A.1), P_1 and P_2 are the partial pressures of water vapor estimated at the membrane surface temperatures T_{hm} and T_{cm}, respectively. The partial pressure in Pa is estimated using the Antoine equation [7,36]:

$$P_1 = \exp\left(23.238 - \frac{3841}{T_{\text{hm}} - 45}\right)\left(1 - C_s\right)\left(1 - 0.5C_s - 10C_s^2\right) \tag{A.2}$$

$$P_2 = \exp\left(23.238 - \frac{3841}{T_{\text{cm}} - 45}\right) \tag{A.3}$$

C_s is the water salinity in percentage. C_m is the membrane distillation (MD) coefficient calculated from three correlations depending on the type of mass transfer regime:

Knudson flow mechanism:

$$C_m^k = \frac{2\varepsilon r}{3\tau\delta}\left(\frac{8M_W}{\pi RT}\right)^{1/2} \tag{A.4}$$

Molecular diffusion mechanism:

$$C_m^d = \frac{\varepsilon}{\tau\delta} \times \frac{PD}{P_a} \times \frac{M_W}{RT} \tag{A.5}$$

Knudsen molecular diffusion transition mechanism:

$$C_m^c = \left[\frac{3}{2} \times \frac{\tau\delta}{\varepsilon r}\left(\frac{\pi RT}{8M_W}\right)^{1/2} + \frac{\tau\delta}{\varepsilon} \times \frac{P_a}{PD} \times \frac{RT}{M_W}\right]^{-1} \tag{A.6}$$

These different regimes depend on the wall collision theory of water molecules, and each regime dominates at

a specific range of values for the mean free path of a water molecule. The heat transfer process occurs in three steps:

- Convection from the feed bulk to the vapor-liquid interface at the membrane surface:

$$q_f = h_f\left(T_h - T_{\text{hm}}\right) \tag{A.7}$$

- Convection from the vapor-liquid interface at the membrane surface to the permeate side:

$$q_p = h_p\left(T_{\text{cm}} - T_c\right) \tag{A.8}$$

where h_f and h_p denote the heat transfer coefficients on the feed and cold stream sides, respectively.

- Evaporation and conduction through the microporous membrane:

$$q_m = JH_v + h_m\left(T_{\text{hm}} - T_{\text{cm}}\right) \tag{A.9}$$

where H_v is the latent heat of water, which can be estimated using Eq. (A.10) [37], whereas h_m is the conductive heat transfer coefficient and is equal to k_m/δ, where k_m and δ denote the membrane-thermal conductivity and its thickness, respectively.

$$H_v\left(T\right) = 1850.7 + 2.8273T - 1.6\times10^{-3}T^2 \tag{A.10}$$

The total heat flux across the membrane is directly proportional to the bulk temperature gradient and can be expressed as follows:

$$Q = U\left(T_h - T_c\right) \tag{A.11}$$

For countercurrent flow, the bulk temperatures are taken as $T_h = T_{h_{\text{in}}}, T_c = T_{c_{\text{out}}}$.

The overall heat transfer coefficient is given by:

$$U = \left[\frac{1}{h_f} + \frac{1}{h_m + \dfrac{JH_v}{T_{\text{hm}} - T_{\text{cm}}}} + \frac{1}{h_p}\right]^{-1} \tag{A.12}$$

Under steady-state operation, the heat transfer in the three individual parts of the system reaches equilibrium:

$$q_f = q_m = q_p \tag{A.13}$$

Considering the macroscopic scale of the MD unit (Fig. (A.1)), the heat balance around the permeate side is given by Eq. (A.14) [38]:

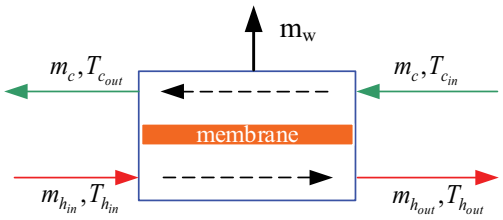

Fig. A.1. Typical DCMD unit.

$$UA_s\left(T_h - T_c\right) = m_c\rho Cp\left(T_{c_{\text{out}}} - T_{c_{\text{in}}}\right) \tag{A.14}$$

where m_c and Cp denote the volume flow rate and specific heat at constant pressure, respectively. Eq. (A.14) is used to compute the permeate exit temperature, $T_{c_{\text{out}}}$. Similarly, assuming a constant density and heat capacity, the mass and heat balance around the feed side are given by:

$$UA_s\left(T_h - T_c\right) = m_{h_{\text{in}}}\rho\text{Cp}\left(T_{h_{\text{out}}} - T_{\text{ref}}\right) - m_{h_{\text{out}}}\rho\text{Cp}\left(T_{h_{\text{in}}} - T_{\text{ref}}\right) \tag{A.15}$$

$$m_{h_{in}} - m_{h_{\text{out}}} = m_W \tag{A.16}$$

Eq. (A.15) is used for computing $T_{h_{\text{out}}}$. It should be noted that Eqs. (A.14) and (A.15) are based on the ideal case where heat losses are negligible. Additional terms can be added to account for heat losses as a percentage of the total heat transfer to achieve congruence between the calculated $T_{c_{\text{out}}}$ and $T_{h_{\text{out}}}$ and the experimental values. The definitions of various variables, the numerical values of the physical and design parameters in Eqs. (A.1)–(A.16), and additional supporting correlations are provided by Safavi and Mahmmadi [39] and Chen and Ho [40].

The key performance index for the MD process, such as the recovery rate and the performance ratio, can also be defined as follows [9,10]:

$$\text{Rc} = \frac{m_w}{m_{h_{\text{in}}}} = \frac{\text{JA}}{m_{h_{\text{in}}}} \tag{A.17}$$

$$\text{GOR} = \frac{H_v}{H_{\text{in}}} = \frac{JA\lambda}{m_{h_{\text{in}}}Cp\left(T_{h_{\text{in}}} - T_{\text{ref}}\right)} \tag{A.18}$$

When the permeate-heat recovery is utilized, the gain output ratio is modified as follows:

$$\text{GOR} = \frac{H_v}{H_{\text{in}}} = \frac{JA\lambda}{m_{h_{\text{in}}}Cp\left(T_{h_{\text{in}}} - T_{c_{\text{out}}}\right)} \tag{A.19}$$